JCI The Journal of Clinical Investigation

Requirement of enhanced Survival Motoneuron protein imposed during neuromuscular junction maturation

Shingo Kariya, … , Shunichi Homma, Umrao R. Monani

J Clin Invest. 2014;124(2):785-800. https://doi.org/10.1172/JCI72017.

Research Article

Spinal muscular atrophy is a common motor neuron disease caused by low survival motoneuron (SMN), a key protein in the proper splicing of genes. Restoring the protein is therefore a promising therapeutic strategy. Implementation of this strategy, however, depends on defining the temporal requirements for SMN. Here, we used controlled knockdown of SMN in transgenic mice to determine the precise postnatal stage requirements for this protein. Reducing SMN in neonatal mice resulted in a classic SMA-like phenotype. Unexpectedly, depletion of SMN in adults had relatively little effect. Insensitivity to low SMN emerged abruptly at postnatal day 17, which coincided with establishment of the fully mature neuromuscular junction (NMJ). Mature animals depleted of SMN eventually exhibited evidence of selective neuromuscular pathology that was made worse by traumatic injury. The ability to regenerate the mature NMJ in aged or injured SMN-depleted mice was grossly impaired, a likely consequence of the inability to meet the surge in demand for motoneuronal SMN that was seen in controls. Our results demonstrate that relative maturity of the NMJ determines the temporal requirement for the SMN protein. These observations suggest that the use of potent but potentially deleterious SMN-enhancing agents could be tapered in human patients once the neuromuscular system matures and reintroduced as needed to enhance SMN for remodeling aged or injured NMJs.

Requirement of enhanced Survival Motoneuron protein imposed during neuromuscular junction maturation

Shingo Kariya,[1,2] Teresa Obis,[3] Caterina Garone,[4,5] Turgay Akay,[2,6] Fusako Sera,[7] Shinichi Iwata,[7] Shunichi Homma,[7] and Umrao R. Monani[1,2,4]

[1]Department of Pathology and Cell Biology and [2]Center for Motor Neuron Biology and Disease, Columbia University Medical Center, New York, New York, USA. [3]Department of Histology and Neurobiology, School of Medicine and Health Sciences, Rovira i Virgili University, Reus, Spain. [4]Department of Neurology, Columbia University Medical Center, New York, New York, USA. [5]Human Genetics PhD Program, Universities of Bologna and Turin, Turin, Italy. [6]Department of Neurological Surgery and [7]Department of Medicine, Columbia University Medical Center, New York, New York, USA.

Spinal muscular atrophy is a common motor neuron disease caused by low survival motoneuron (SMN), a key protein in the proper splicing of genes. Restoring the protein is therefore a promising therapeutic strategy. Implementation of this strategy, however, depends on defining the temporal requirements for SMN. Here, we used controlled knockdown of SMN in transgenic mice to determine the precise postnatal stage requirements for this protein. Reducing SMN in neonatal mice resulted in a classic SMA-like phenotype. Unexpectedly, depletion of SMN in adults had relatively little effect. Insensitivity to low SMN emerged abruptly at postnatal day 17, which coincided with establishment of the fully mature neuromuscular junction (NMJ). Mature animals depleted of SMN eventually exhibited evidence of selective neuromuscular pathology that was made worse by traumatic injury. The ability to regenerate the mature NMJ in aged or injured SMN-depleted mice was grossly impaired, a likely consequence of the inability to meet the surge in demand for motoneuronal SMN that was seen in controls. Our results demonstrate that relative maturity of the NMJ determines the temporal requirement for the SMN protein. These observations suggest that the use of potent but potentially deleterious SMN-enhancing agents could be tapered in human patients once the neuromuscular system matures and reintroduced as needed to enhance SMN for remodeling aged or injured NMJs.

Introduction

Lesions in the survival of motor neuron 1 (*SMN1*) gene underlie the common and often fatal pediatric neuromuscular disorder spinal muscular atrophy (SMA) (1). The disease, defined primarily by spinal motor neuron loss, is one of the most frequently (~1:6400 newborns) inherited causes of infant mortality (2, 3). Yet no effective SMA treatment currently exists, and available therapies remain little more than palliative. SMA is caused by the homozygous loss of the *SMN1* gene, but patients invariably retain 1 or more copies of an almost identical homologue, *SMN2*. This gene fails to fully protect against *SMN1* loss owing to a translationally silent exon 7 C→T nucleotide substitution that creates an exonic splicing suppressor disrupting proper splicing (4–6). Consequently, most *SMN2* transcripts lack exon 7 and are translated into a protein (SMNΔ7) that is unstable and degraded. Accordingly, SMA is characterized by low SMN levels (7, 8) that appear to have a particularly detrimental effect on the motor system.

Although the *SMN2* gene expresses only a fraction of the functional SMN protein produced by its homolog, sufficient copies can mitigate disease severity in SMA model mice as well as human patients (9–12). Modulating *SMN2* expression to enhance the SMN protein and treat SMA is therefore a central therapeutic strategy (13, 14). In SMA model mice, antisense oligonucleotides (ASOs) that correct the splicing defect of the *SMN2* gene and restore SMN protein show remarkable benefit (15, 16). Equally effective is recombinant adeno-associated virus (AAV9), engineered to replace mutant SMN genes with functional copies (17–20). Yet owing to current limitations in biodistribution of AAV9 or ASOs to the CNS of large animals, emerging treatment strategies involve invasive intrathecal administrations designed to target motor neurons. Considering the fragility of most SMA patients, such invasive treatment regimens may not be the preferred choice for clinicians or their patients. Intrathecal administration of these agents also precludes targeting potentially critical cellular sites of action of the SMN protein that lie outside the nervous system. One attractive alternative involves the use of orally administered, blood-brain penetrating small molecule enhancers of SMN. However, since small molecules are often associated with long-term, off-target side effects, their use will have to be carefully calibrated. Doing so safely and effectively using these, or indeed any modulator of *SMN2* expression, requires a clear understanding of the spatial and temporal requirements for the SMN protein.

Previous investigations of the temporal requirements for the SMN protein have demonstrated that while restoring protein to animal models is undoubtedly therapeutic in nature, it is most effective early in the disease and during a relatively brief window in time (21, 22). A decline in the ability to halt or reverse the disease correlated with an accumulation of neuromuscular synaptic defects, suggesting that the therapeutic window is defined by a period encompassing neuromuscular system maturation. One prediction that follows from this observation is a stringent but temporally limited requirement for the protein during neuromuscular synapse maturation. The discovery of profoundly immature neuromuscular junctions (NMJs) in model mice depleted either

Conflict of interest: The authors have declared that no conflict of interest exists.
Citation for this article: *J Clin Invest.* 2014;124(2):785–800. doi:10.1172/JCI72017.

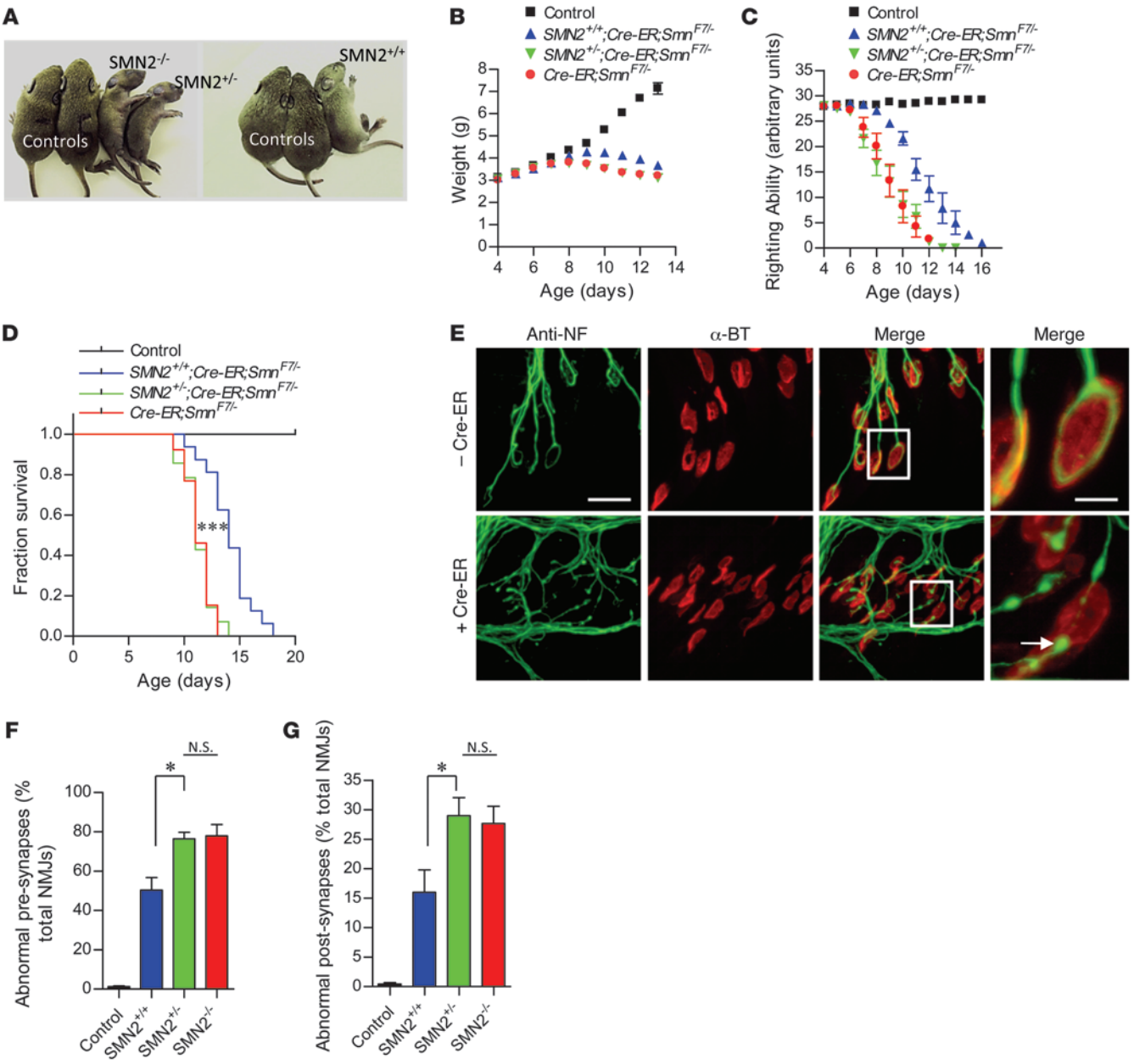

Figure 1

Severe neuromuscular disease in mice depleted of SMN during neonatal life. (**A**) Characteristic paralytic phenotype of P11 0-copy (*SMN2*$^{-/-}$), 1-copy (*SMN2*$^{+/-}$), or 2-copy (*SMN2*$^{+/+}$) *CreER;Smn*$^{F7/-}$ mutants treated with TM at 4 days of age. Decline in (**B**) body weight, (**C**) righting ability, and (**D**) survival during the first 2 weeks following SMN depletion characterizes the onset and progression of neuromuscular disease in the mutants. Two *SMN2* copies partially mitigate disease, slowing the loss of body weight, improving motor performance, and enhancing survival. $n \geq 10$ (**B** and **C**) and $n \geq 13$ (**D**) mice of each genotype for analyses. ***$P < 0.0001$, log-rank test. (**E**–**G**) Evidence of abnormal NMJs in 0, 1-, or 2-copy *SMN2* mice depleted of SMN protein. NMJs in **E** are from 2-copy *SMN2* mutants but are illustrative of the defects seen in all 3 cohorts of SMA mice. Arrow depicts NF-containing varicosity at nerve terminal. NMJ analysis was conducted on $n \geq 900$ synapses from $n \geq 3$ mice of each genotype. *$P < 0.05$, 1-way ANOVA. Note that in every case, controls are 2-copy *SMN2;Smn*$^{F7/-}$ mice lacking the *CreER* transgene. Scale bars: 38 μm; 10 μm (inset).

ubiquitously or selectively in motor neurons for SMN supports this notion (23–26). Still, these models were depleted of SMN from the earliest time points, making it difficult to ascertain the cellular, pathologic, and phenotypic consequences of protein loss specifically during postnatal and adult stages of life. Such information is of dual significance. First, it directly addresses the question, are there alterations in the postnatal requirements of mammalian organisms for a housekeeping protein involved in the biogenesis of spliceosomal snRNP particles? An answer to this question informs our understanding of the relative requirements for the vitally important processes of snRNP biogenesis and pre-mRNA splicing in diverse cell types during postnatal development and adult

life. The rapid but somewhat delayed postnatal onset of the SMA phenotype in mice (27) and especially patients reported to have normal motor unit numbers (28, 29) may indeed reflect a stage-dependent requirement of 1 or more cells of the neuromuscular system for biological functions of SMN such as snRNP biogenesis and pre-mRNA splicing in ensuring their proper development. Second, and of more immediate clinical relevance, such information facilitates the design of truly safe and effective treatments for human SMA. For instance, it enables the calibration of drug doses for patients treated chronically with potent concentrations of *SMN2*-enhancing molecules that possess real or potentially adverse long-term effects.

Here we have used what we believe to be a novel line of *SMN2*-expressing transgenic mice to precisely define the postnatal requirements for the SMN protein. Depleting SMN in neonatal mice produced a classic SMA-like phenotype, whereas depleting the protein to equivalent levels in adult mice produced no overt disease for many months. However, recovery of muscle or motor nerves, but not skin, was impaired following injury. Furthermore, the reestablishment of mature neuromuscular synapses following motor nerve injury induced a sharp increase in motor neuronal SMN expression that could not be effected in *Smn*-inactivated animals. Experiments to determine when SMN-depleted mice became resistant to low protein revealed that the transition occurred concomitant with the establishment of the fully mature neuromuscular synapse. We conclude that the relative requirements for the SMN protein are radically altered during postnatal life, declining once the NMJ matures but rising again if the synapse sustains injury. This implies that treatment of SMA with enhancers of *SMN2* expression will have to be at its most aggressive during the maturation of the neuromuscular system, but that drug doses may be diminished thereafter without precipitating a severe disease phenotype.

Results

Neonatal depletion of the SMN protein precipitates a severe neuromuscular disease phenotype. SMA model mice with 2 *SMN2* copies on a null murine *Smn* background develop a severe and invariably fatal neuromuscular disease (9). To determine the effects of delaying SMN depletion to postnatal life, we generated *SMN2*-expressing mice harboring a floxed murine *Smn* allele (Smn^{F7}) that can be inactivated following Cre-mediated recombination (30). We further introduced onto this genetic background an *Smn*-null allele (31) and a ubiquitously expressed tamoxifen-inducible (TM-inducible) *CreEr* transgene (32). Since the floxed allele expresses wild-type SMN levels, untreated transgenic *(SMN2;CreER;*$Smn^{F7/-}$*)* mice are disease free and phenotypically no different from $Smn^{+/-}$ heterozygotes. By modifying our breeding scheme, we were able to generate *CreER;*$Smn^{F7/-}$ animals carrying 0 (–/–), 1 (+/–), or 2 (+/+) *SMN2* copies.

Depleting SMN by administering TM to P4 *CreER;*$Smn^{F7/-}$ animals homozygous for *SMN2* rapidly induced an SMA-like disease phenotype characterized by loss of body weight, impaired motor performance, and eventual paralysis (Figure 1, A–C). Death quickly followed, and none of the mutants survived beyond P17 (Figure 1D). Abolishing SMN is incompatible with cell survival and embryonic lethal to mice (30). Accordingly, TM-treated *CreER;*$Smn^{F7/-}$ mice lacking the *SMN2* gene developed an even more severe disease phenotype (Figure 1, A–C) and survived significantly fewer days than their *SMN2* homozygous cohorts (Figure 1D). Interestingly, a single *SMN2* copy failed to mitigate the disease phenotype observed in TM treated *CreER;*$Smn^{F7/-}$ mice (Figure 1, B–D), suggesting that during neonatal life, at least 2 *SMN2* copies are required to bring about a discernible modification of the disease phenotype.

To quantify the effects of administering TM at P4 on SMN protein levels, we subjected lumbar spinal cords of 2-copy *SMN2;CreER;*$Smn^{F7/-}$ mice to immunohistochemical analysis 8 days after treatment. SMN in the motor neuron soma of these mice was virtually undetectable (Supplemental Figure 1A; supplemental material available online with this article; doi:10.1172/JCI72017DS1) and gems, SMN-containing nuclear foci often used to quantify protein levels (7), in these cells were reduced to approximately 10% of those observed in motor neurons of similarly genotyped mice without the *CreER* transgene (Supplemental Figure 1B). Consistent with this result, SMN in whole spinal cord, skeletal muscle, and heart was dramatically reduced (Supplemental Figure 1C). Considering the depletion of SMN in the motor neurons of the treated mutants, we were interested to find that there was no significant loss of these cells (Supplemental Figure 1E). We therefore examined the NMJs of the mutants, which showed early pathology in response to low SMN (33). We found that the NMJs displayed defects of both pre- and postsynaptic regions. Presynaptic regions at the NMJs terminated as end bulbs, globular structures infiltrated with neurofilament protein. Postsynaptic regions of the NMJs were characterized by poorly staining (AChR) clusters, evidence of receptor disassembly (Figure 1, E–G, and Supplemental Figure 1E). NMJs of *CreER;*$Smn^{F7/-}$ mutants bearing 0 or 1 *SMN2* copy were similarly or even more significantly affected, whereas those of mice without the *CreER* transgene appeared normal (Figure 1, F and G).

SMA model mice expressing constitutively low SMN not only develop a neuromuscular phenotype, but also severe cardiac defects (34–36). We therefore used highly sensitive echocardiography to investigate the possibility of cardiac dysfunction in P13 2-copy *SMN2;CreER;*$Smn^{F7/-}$ mice and relevant controls administered TM on day 4. To our surprise, cardiac function as determined by heart rate, fractional area change, and cardiac index was not adversely affected in SMN-depleted mutants (Supplemental Figure 2, A–D). In contrast and as previously reported, P11 "SMNΔ7" SMA mice, a commonly used model of the disease, *did* exhibit evidence of cardiac dysfunction. Collectively, these results lead us to the following important conclusions: first, there is a continued requirement for normal levels of the SMN protein during early postnatal life. Inducing low levels in heterozygous mice that develop normally nevertheless brings about an SMA-like phenotype. Second, it is the neuromuscular system in these mutants that appears to be selectively vulnerable to low SMN, as the heart, a second organ reported to be affected relatively early in SMA mice and some patients (37), did not exhibit evidence of dysfunction. Finally, we confirm previous studies demonstrating that the neuromuscular system is initially affected at the distal motor unit, the NMJ, in response to low SMN protein.

A transition to adult life confers a remarkable protective effect against SMN protein loss. To determine whether the requirements for SMN are altered once the organism matures, we investigated the effects of depleting protein at P50 in 0-, 1-, and 2-copy *SMN2;CreER;*$Smn^{F7/-}$ mice. We began by treating P50 *CreER;*$Smn^{F7/-}$ mice with TM to assess the efficiency with which we were able to deplete SMN. Our experiments showed that pro-

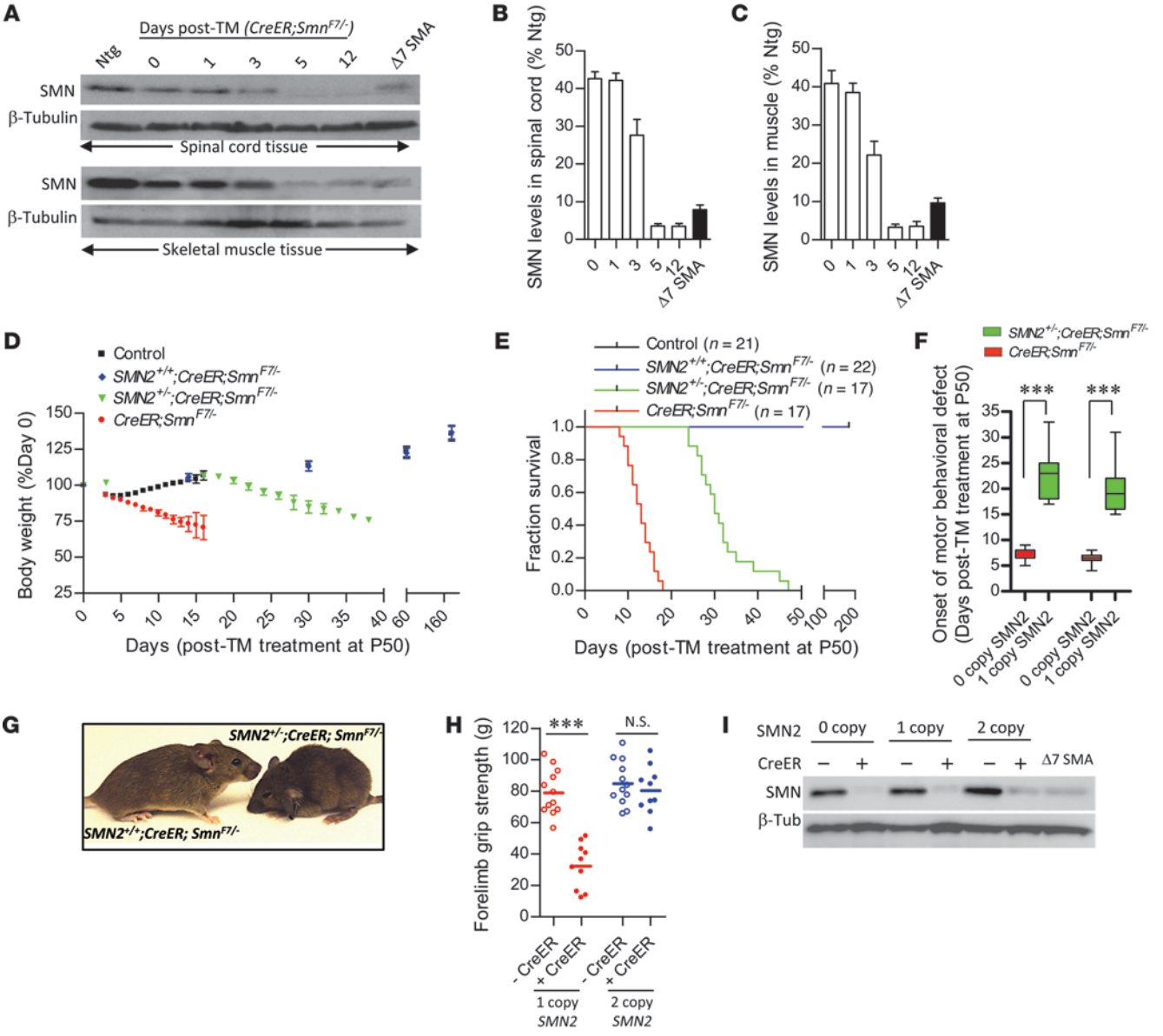

Figure 2

An SMN-resistant state is acquired during adult life. (**A**) Western blot analysis of SMN in tissues of inducible mice demonstrates dramatic depletion of protein 5 days following TM administration. Quantification of protein levels in (**B**) spinal cord and (**C**) skeletal muscle of treated mutants at the various time points examined. $n \geq 3$ mice analyzed for each time point. (**D**) Loss of body weight and (**E**) early mortality of SMN-depleted mutants harboring 0 or 1 but not 2 *SMN2* copies. (**F**) A delay in the onset of disease in mice bearing 1 versus 0 copies of the *SMN2* gene. $^{***}P < 0.001$, *t* test, $n \geq 10$ mice. (**G**) Representative image of 1- and 2-copy *SMN2* inducible mutants 30 days following TM administration depict an alert, relatively healthy $SMN2^{+/+}$ mouse compared with its hunched and somewhat disheveled looking hemizygous ($SMN2^{+/-}$) littermate. (**H**) Two- but not one *SMN2* copy in SMN-inducible mice protects against loss of forelimb strength. $^{***}P < 0.001$, *t* test, $n \geq 12$ mice of each genotype. (**I**) Western blot depicting robust and equivalent depletion of SMN protein in the various cohorts of inducible mutants.

tein levels in the spinal cords and gastrocnemius muscle of the mice dropped to approximately 40%, 25%, and 5% of wild-type levels 1, 3, and 5 days after treatment, respectively (Figure 2, A–C), suggesting relatively efficient inactivation of the *Smn* gene. Indeed, depletion eventually exceeded that observed in SMNΔ7 SMA mice. Similar efficiencies were observed in heart, kidney, and liver tissues (Supplemental Figure 3, A and B), consistent with the ubiquitous expression of the *CreER* transgene.

We next focused on the phenotypic effects of the SMN depletion. As expected, $CreER;Smn^{F7/-}$ mutants quickly became symptomatic of disease, lost weight, and were moribund within approximately 13 days of TM treatment (Figure 2, D and E). A single *SMN2* copy was found to confer significant ($P < 0.001$) benefit to TM-treated $CreER;Smn^{F7/-}$ mice, a contrast to our observations in neonates. In such animals, disease onset as measured by motor performance in the vertical pole and rotarod tests was delayed, and survival

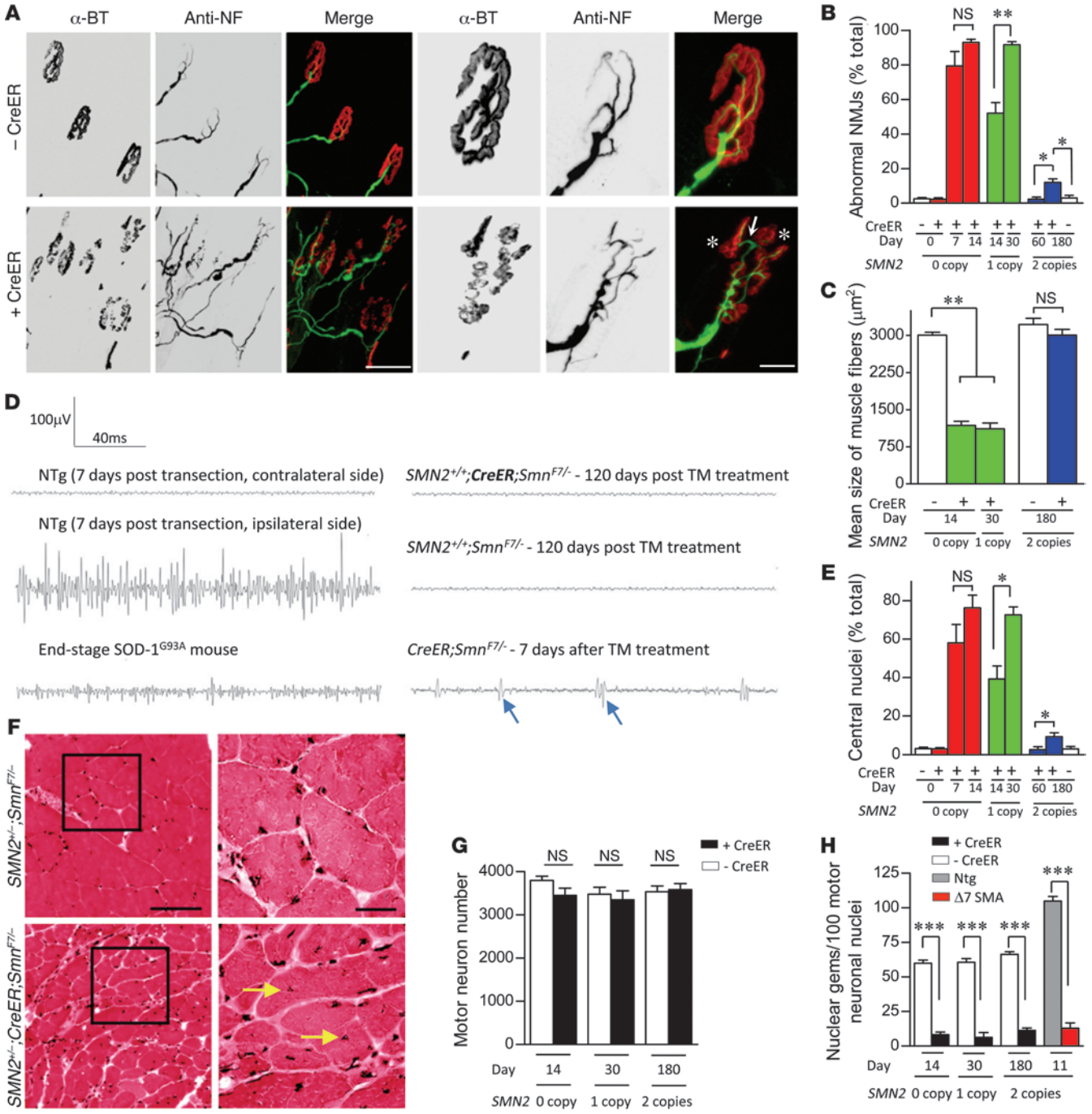

Figure 3

Age-dependent emergence of NMJ and muscle pathology in SMN-depleted mutants. (**A**) Immunostains of NMJs in the gastrocnemius muscle of end-stage 0- or 1-copy *SMN2* inducible mutants revealed profound abnormalities including AChR cluster fragmentation (asterisks) and imperfect overlap between pre- and postsynaptic regions (arrow). Depicted are NMJs from a TM-administered *CreER;Smn*$^{F7/-}$ mouse and a control without the *CreER* transgene. Scale bars: 100 μm; 30 μm (detail). (**B**) Quantification of NMJ defects in 0-, 1-, and 2-copy *SMN2*-inducible mutants. *$P < 0.05$; **$P < 0.01$. $n = 300$ NMJs from each of 3 mice of each genotype, 1-way ANOVA. (**C**) Normal muscle fiber size in the gastrocnemius of homozygous *SMN2* but not hemizygous or 0-copy *SMN2* inducible mice is indicative of relatively normal innervations in the presence of 2 *SMN2* copies. **$P < 0.01$, 1-way ANOVA. $n > 50$ fibers from each of 3 or more mice of each genotype. (**D**) Representative EMG traces recorded from the gastrocnemius muscle of 2-copy *SMN2*-inducible mutants and relevant controls. No evidence of denervation was detected. Shown are fibrillation potentials (arrows), a sign of denervation in *CreER;Smn*$^{F7/-}$ mutants, end-stage SOD-1^{G93A} ALS model mice and animals in which the sciatic nerve was transected. (**E**) Extent of centrally nucleated myofibers in the various cohorts of SMN-inducible mutants. Statistics calculated as in **C**. (**F**) H&E stains of gastrocnemius muscle in transverse section are illustrative of a primary myopathy in the SMN-inducible mice; arrows indicate central nuclei. Scale bars: 100 μm; 30 μm (inset). Quantification of (**G**) motor neurons and (**H**) motor neuronal gems failed to provide evidence of cell loss despite profound SMN depletion. Motor neurons and gems in each of 3 mice of the various genotypes were quantified. ***$P < 0.001$, *t* test.

significantly enhanced to approximately 30 days after treatment (Figure 2, D–F). However, we were struck by the effect of placing 2 *SMN2* copies on the *CreER;Smn*$^{F7/-}$ background. To our surprise, TM treatment of these mice produced little evidence of overt disease compared with the effects seen in 1-copy *SMN2;CreER;Smn*$^{F7/-}$ mutants (Figure 2G and Supplemental Video 1). Moreover, like controls that lacked the *CreER* transgene and therefore expressed normal SMN, these mutants continued to gain weight and invariably survived to at least 8 months of age (Figure 2, D and E, and Supplemental Figure 4). Results of a grip-strength test conducted on these animals approximately 120 days after TM administration were consistent with the absence of a disease phenotype. Two-copy *SMN2;CreER;Smn*$^{F7/-}$ mice depleted of SMN performed just as robustly as controls expressing normal protein (Figure 2I). In contrast, 1-copy *SMN2;CreER;Smn*$^{F7/-}$ mice subjected to this test 25 days following treatment were profoundly weak relative to their normal SMN-expressing controls (Figure 2H). To ensure that the different phenotypes observed in 0-, 1-, and 2-copy *SMN2;CreER;Smn*$^{F7/-}$ mice were not simply a consequence of variable SMN depletion, we assessed protein levels in the spinal cords of the animals 2 weeks following TM administration. In every instance, SMN was dramatically reduced and comparable to levels observed in the spinal cord of a P14 SMNΔ7 SMA mouse (Figure 2I). In aggregate, these results imply the acquisition, at adult stages, of a remarkable resistance to low SMN and suggest a dramatic decline in the minimum levels of protein required for normal function. Importantly, this resistance is acquired with a minimum of 2 *SMN2* copies, the same number found in most SMA patients (12) and therefore of direct relevance to treating the human disease.

Neuromuscular system selectively affected in aging, SMN2-expressing mice depleted of the SMN protein. To determine whether the apparent resistance of adult mice to SMN depletion extended beyond an overtly normal phenotype, we subjected TM treated 0-, 1-, and 2-copy *SMN2;CreER;Smn*$^{F7/-}$ mice to a comprehensive pathologic analysis. We began by examining the NMJs. Synapses of *CreER;Smn*$^{F7/-}$ mice bearing 0 or 1 *SMN2* copy were clearly abnormal, consisting of poorly stained, disassembled, or fragmented AChR clusters (Figure 3A). This became worse with time until practically all of the NMJs bore defects (Figure 3B). In contrast, we found no morphological defects in the NMJs of *CreER;Smn*$^{F7/-}$ mutants bearing 2 *SMN2* copies 2 months after TM treatment (Figure 3B and Supplemental Figure 5A). Interestingly, an examination of the NMJs 6 months after treatment at, approximately P230, did reveal pathology, but this was limited to approximately 15% of the total synapses analyzed (Supplemental Figure 5A). One implication of this observation is that, notwithstanding the absence of overt disease, effective maintenance of the NMJs in aging mice depleted of SMN is compromised. Nevertheless, we were unable to detect significant evidence of denervation at this time point either in the form of muscle atrophy (Figure 3C) or by electromyographic (EMG) means (Figure 3D), consistent with the observation of normal motor activity in the animals. *CreER;Smn*$^{F7/-}$ mutants with 0 or 1 *SMN2* copy, on the other hand, had markedly smaller muscle fibers and exhibited evidence of fibrillation potentials toward the end of the disease, clear indications of functional denervation. Muscle fibers of these mice were furthermore characterized by widespread centrally rather than peripherally located nuclei, whereas this distinct pathology, a sign of a primary muscle disease, only became significant in the 2-copy *SMN2* mutants at approximately P230 (Figure 3, E and F). To determine the effects of SMN depletion in the motor neuron cell bodies of the 3 mutants, we counted motor neurons and quantified gems in them. In no instance did we detect a significant loss of the spinal motor neurons in the treated animals (Figure 3G), despite a profound depletion of SMN gems (Figure 3H) and protein in the soma of the cells (Supplemental Figure 5B). Together, these results suggest that 2 *SMN2* copies not only prevent overt disease in adult mice depleted of the SMN protein, but also protect the neuromuscular system from SMA pathology. The eventual appearance, albeit modest, of NMJ defects and muscle fiber pathology suggests that the long-term maintenance of motor neurons and muscle is compromised in the absence of sufficient SMN. Still, the absence of any motor neuron loss in any of the mutants implies that, whereas the cells may acquire defects, they do not altogether degenerate.

To determine whether other organ systems are spared to a similar or even greater extent in aging TM-treated 2-copy *SMN2;CreER;Smn*$^{F7/-}$ mice, we first used echocardiography to examine heart function. Measurements of heart rate, oxygen saturation (SpO_2), and cardiac output in P200–P220 mutants were no different than those of controls (Supplemental Figure 6, A–C). Fractional area changes, a measure of cardiac contractility and left ventricular anterior wall thickness indicative of myocardial function, were also found to be equivalent in mutants and controls (Supplemental Figure 6, D–F). Interestingly, similar measurements in *CreER;Smn*$^{F7/-}$ mice 7 days after treatment, when NMJ defects were unmistakable, showed that the heart was normal in these mutants too (Supplemental Figure 7, A–G). Defects only became obvious 10 days or more after treatment. Collectively, these results suggest that 2 *SMN2* copies are sufficient to protect against cardiac dysfunction even in aging mice depleted of SMN during adult life. They furthermore confirm the early, selective vulnerability of the neuromuscular system to low SMN.

An analysis of circulating blood cells and serum proteins is a sensitive way to detect disease and dysfunction in various organ systems. Accordingly, we also quantified blood cell numbers, serum AST, ALT, and bilirubin (enzymes indicative of liver function), blood urea nitrogen/creatine (a measure of kidney function), lipase (a measure of pancreatic function), creatine kinase (CK) (a measure of muscle function), and LDH (a measure of cardiac function and tissue breakdown), among other parameters in 5.5-month TM-treated 2-copy *SMN2;CreER;Smn*$^{F7/-}$ mice. Mutant parameters were found to be no different from those of controls with normal SMN (Supplemental Figure 8, A and B), further indication of the general protective effect of a transition to adulthood against low protein. In contrast and as expected, multiple signs of disease characterized by inflammatory white blood cells and abnormal CK levels emerged as early as 7 days following treatment of *CreER;Smn*$^{F7/-}$ mice (Supplemental Figure 8, A and B).

Stringent requirement for elevated SMN protein during neuromuscular synapse maturation. The emergence of subtle NMJ defects approximately 180 but not 60 days following SMN depletion in adult, 2-copy *SMN2;CreER;Smn*$^{F7/-}$ mice suggested that low protein prevents the repair and regeneration of mature neuromuscular synapses damaged during the normal process of aging (38). We hypothesized that such defects would become even more prominent in response to focal damage of the NMJs in older, SMN-depleted animals. To test this hypothesis, we resorted to a sciatic nerve-crush injury paradigm in TM-treated 2-copy *SMN2;Smn*$^{F7/-}$ mice with or without the *CreER* transgene. Following injury, axons distal to the crush site rapidly degenerated, and by day 6, synapses were completely dener-

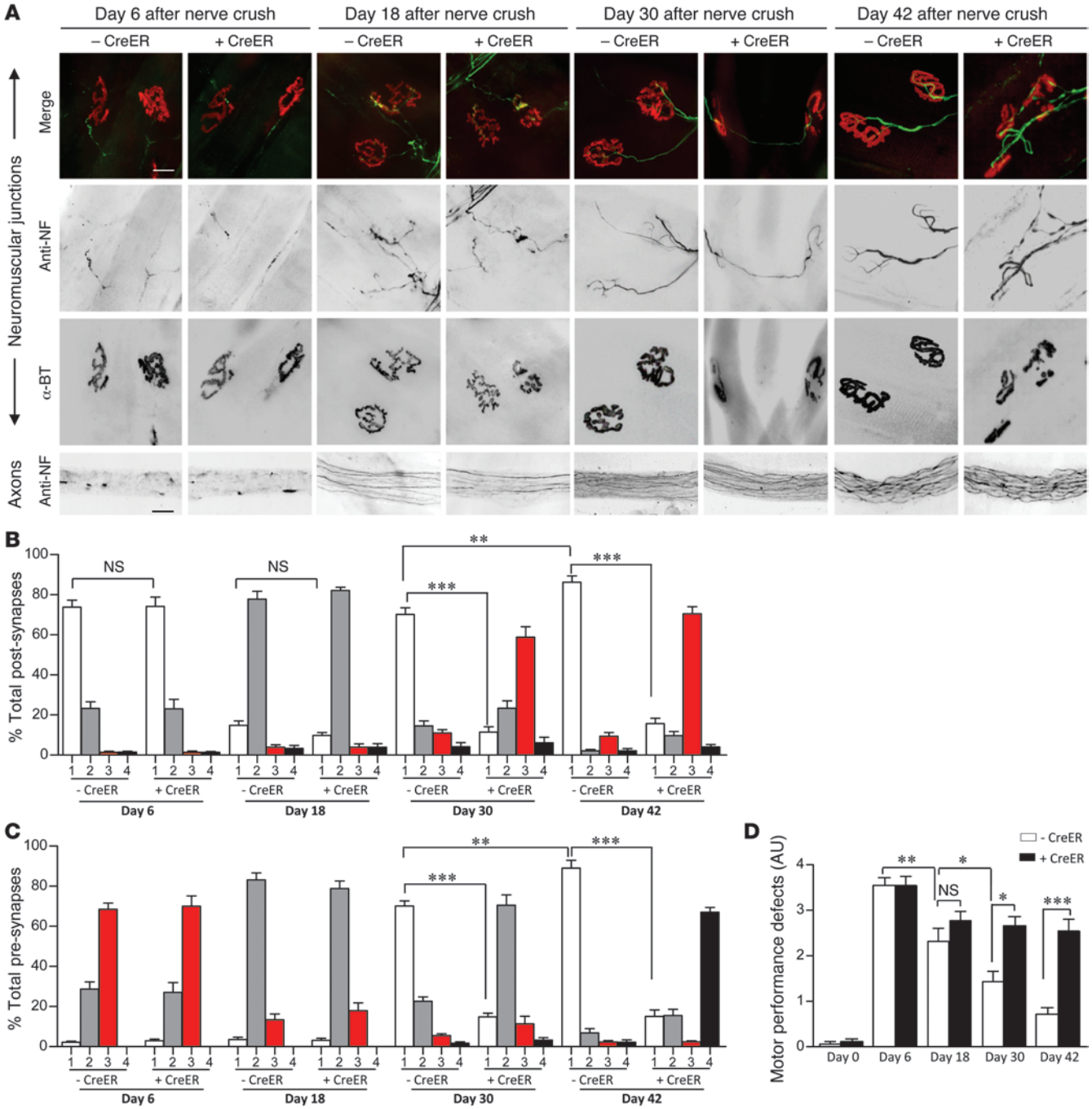

Figure 4

An increased SMN requirement during NMJ maturation. (**A**) Immunostains of the NMJs and distal sciatic nerve axons of treated 2-copy *SMN2;Smn*$^{F7/-}$ mutants with or without the *CreER* transgene at 4 time points following nerve crush. Scale bars: 25 μm. Morphological analysis of (**B**) post- and (**C**) presynaptic specializations of the mice during axon regeneration and NMJ remodeling. n = 1500 NMJs from 5 mice of each genotype. (**D**) An assessment of motor performance following nerve crush indicates a significant difference in recovery between mutants expressing normal and disease-causing levels of SMN. $n \geq 6$ mice tested for the analysis. *$P < 0.05$; **$P < 0.01$; ***$P < 0.001$, 1-way ANOVA.

vated in both sets of mice (Figure 4A). Pre- and postsynaptic regions arbitrarily defined as class 1, 2, 3, or 4 depending on the extent of nerve terminal pathology and AChR disruption (see Methods and Supplemental Figure 9A) did not differ significantly in animals with or without normal SMN (Figure 4, B and C). By day 18, AChR disassembly was evident in both sets of mice, but axons had begun regenerating, defining a period of synapse reinnervation. Synapse distribution between the 4 classes (classes 1–4) did not differ at this stage either, suggesting that reinnervation proceeds normally even in the absence of normal SMN. However, by day 30, whereas most

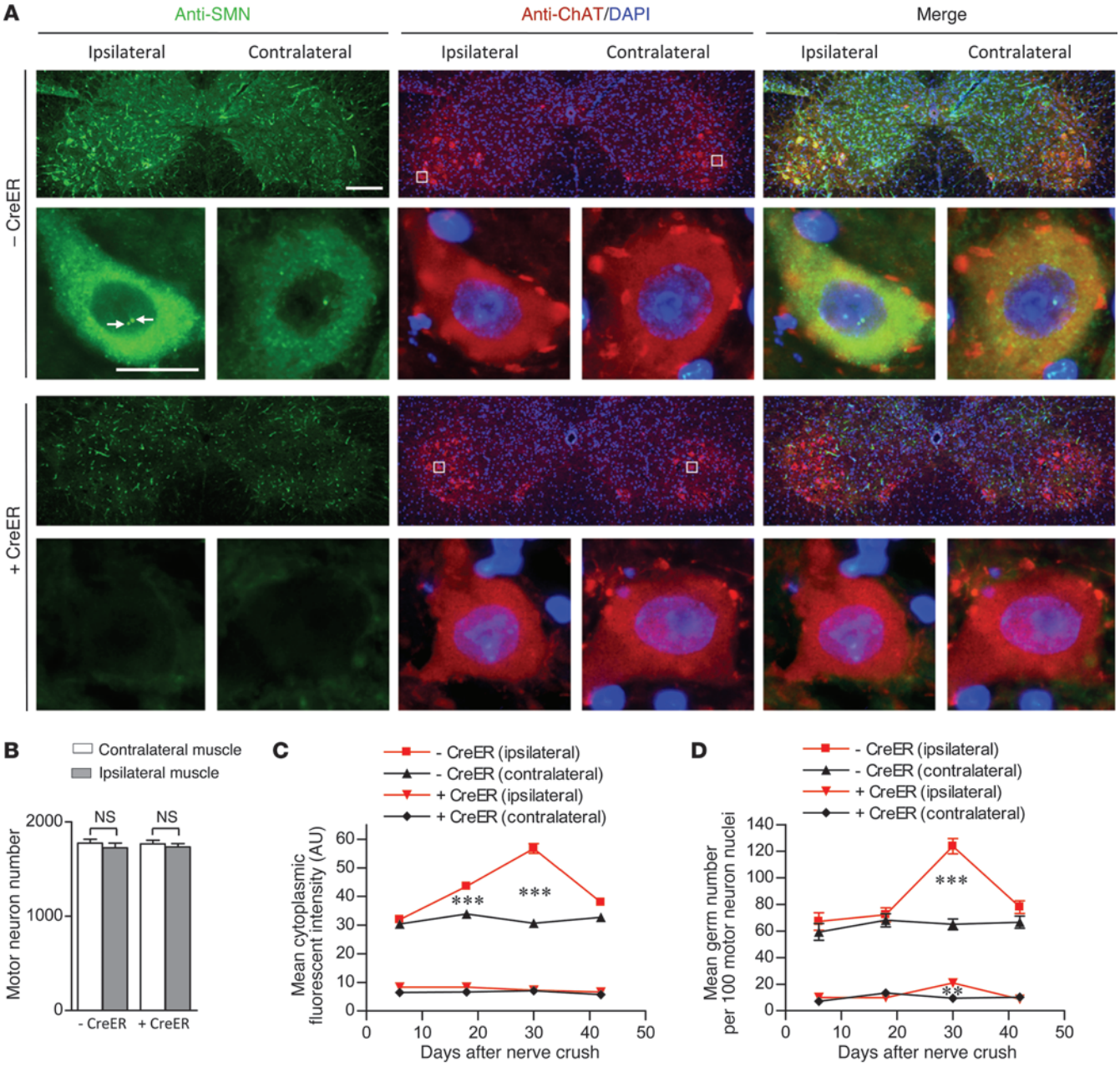

Figure 5

An elevated demand for motor neuronal SMN as disrupted NMJs remodel and mature. (**A**) Immunostains of spinal cord sections from TM-treated 2-copy *SMN2;Smn*$^{F7/-}$ mice with or without the *CreER* transgene 30 days following nerve crush. An elevation in the number of gems (arrows) and cytoplasmic SMN is evident in ipsilateral motor neurons of the *CreER* spinal cord. Scale bars: 240 μm; 30 μm (detail). (**B**) Quantification of motor neurons in the cords of the mice failed to reveal evidence of cell loss. $n \geq 3$ mice of each genotype, *t* tests. However, (**C**) cytoplasmic SMN levels and (**D**) nuclear gems of the ipsilateral motor neurons rose following the nerve crush. Especially evident is the increase which peaks at day 30 after the crush in the *CreER*-negative animals. Cytoplasmic SMN staining in at least 150 motor neurons from 3 mice of each cohort was assessed; ≥ 300 nuclei were examined for gems. $^{**}P < 0.01$; $^{***}P < 0.001$, 1-way ANOVA for the analyses.

NMJs of controls had assumed a normal, mature morphology characterized by elaborately branched nerve terminals perfectly apposed to intensely staining, pretzel-shaped AChR clusters, synapses in animals depleted of SMN remained fragmented and incompletely innervated, mostly by threadlike axon terminals. An analysis of the 2 sets of mice 42 days after nerve injury revealed that approximately 90% of the control NMJs had resumed their normal architecture. In contrast, the maturation of SMN-depleted NMJs remained arrested, characterized once again by small, fragmented AChR clusters and poorly branched nerve terminals, many with numerous varicosities swollen with neurofilament protein (Figure 4, A–C, and Supplemental Figure 9A). These results suggest that whereas axon regeneration,

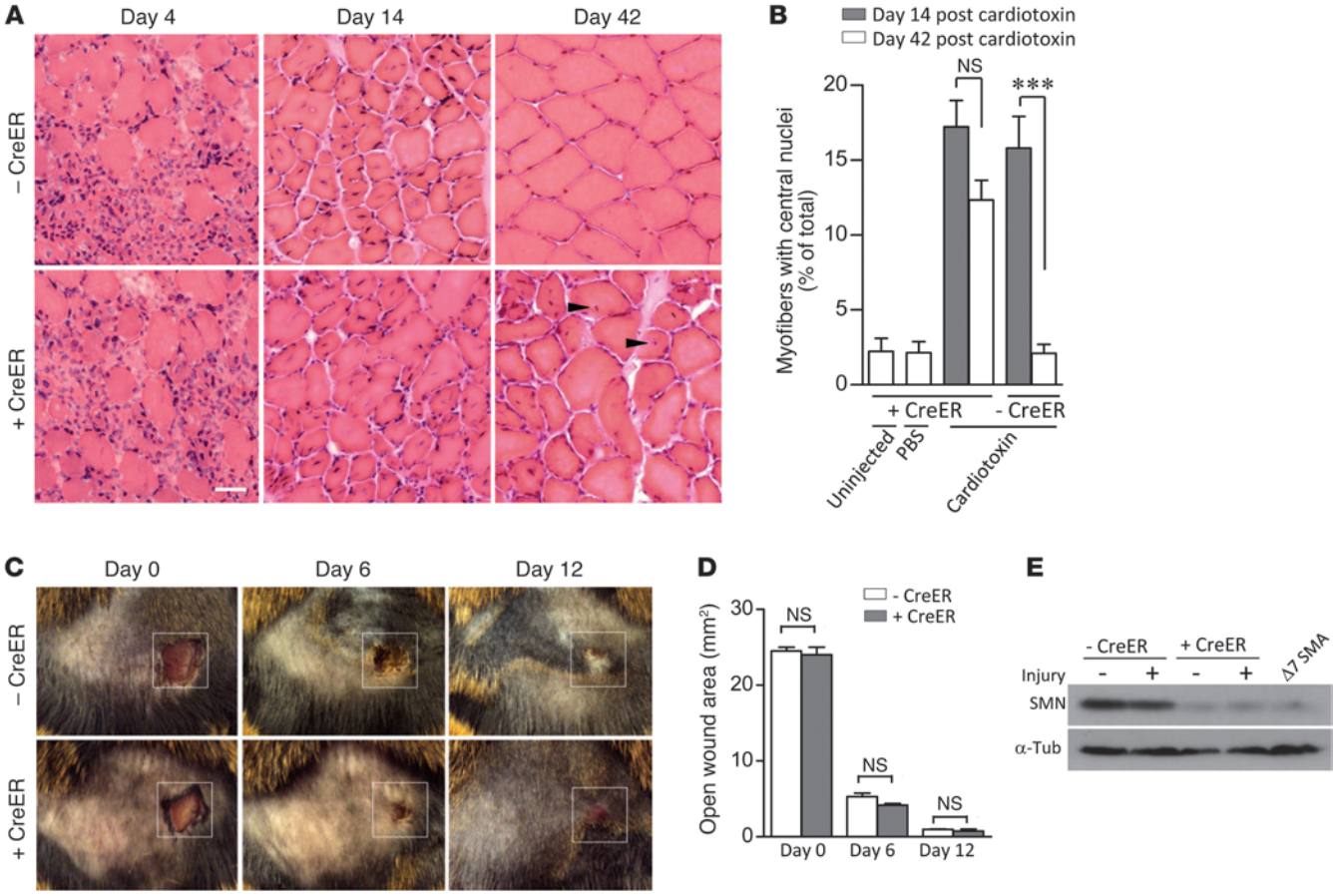

Figure 6

An enhanced requirement for the SMN protein following tissue injury is restricted to the neuromuscular system. (**A**) H&E stains of the gastrocnemii muscles of TM-treated 2-copy *SMN2;Smn*$^{F7/-}$ mice with or without *CreER* reveals an impaired ability of SMN-depleted muscle to fully recover from cardiotoxin injury — see central nuclei (arrowheads) in *CreER* positive muscle. Scale bar: 30 μm. (**B**) Quantification of centrally nucleated myofibers in the 2 sets of mice at days 14 and 42 after -cardiotoxin injection. ***$P < 0.001$, 1-way ANOVA; muscle fibers from $n \geq 5$ mice were examined. (**C**) Recovery from a surface wound to the skin is not compromised by low SMN. Original magnification, ×1. (**D**) Assessment of open wound area in the presence of absence of normal SMN failed to reveal differences at any of the time points examined. $n \geq 3$, *t* test. (**E**) Western blot analysis of SMN from the wound area did not indicate an increase in protein relative to the contralateral area.

outgrowth, and initial contact with muscle following denervation proceeds normally even in the absence of normal SMN, the final assembly, elaboration, and maturation of the NMJ is arrested.

To ascertain whether the inability to fully regenerate mature, morphologically normal NMJs resulted in impaired muscle function, we tested motor performance in the injured animals 6, 18, 30, and 42 days after nerve crush. We found that movement of the ipsilateral hind limbs of the mice was profoundly affected at day 6 irrespective of whether the animals expressed reduced or normal SMN. In contrast, by day 42, limb function of controls expressing normal SMN was largely restored, whereas movement and locomotion of mutants with reduced protein remained impaired, at levels observed on day 18 (Figure 4D and Supplemental Video 2). The inability of injured mutants depleted of SMN to regenerate mature NMJs or recover normal function of the affected limb was furthermore reflected in atrophy of the ipsilateral gastrocnemius, as evidenced by reduced muscle weight (Supplemental Figure 9B) and significantly smaller muscle fibers relative to those of the contralateral muscle (Supplemental Figure 9, C and D). Thus, morphological evidence of arrested NMJ maturation following focal disruption of the synapses of SMN-depleted mutants did indeed have a physiological correlate in muscle function.

To further explore how low SMN stalls the maturation of the NMJ, we examined motor neuron morphology in the lumbar spinal cords of mutant and control mice. We found that there was no motor neuron loss following nerve crush, even at day 42 in SMN-depleted mice (Figure 5, A and B). However, to our surprise, SMN levels in the motor neurons of injured control mice began rising and peaked 30 days after the injury, just as NMJs entered the final phase of AChR elaboration before assuming their fully mature state (Figure 5, A and C). This enhanced immunofluorescence subsided by day 42 approximately to levels observed in contralateral motor neurons. Quantification of gems in the motor neurons over this time period mirrored the increase of cytoplasmic SMN (Figure 5D). In contrast to this global change of motor neuronal SMN following injury to control animals, we observed a discernible increase of only the nuclear gems in the motor neurons of injured, SMN-depleted mutants

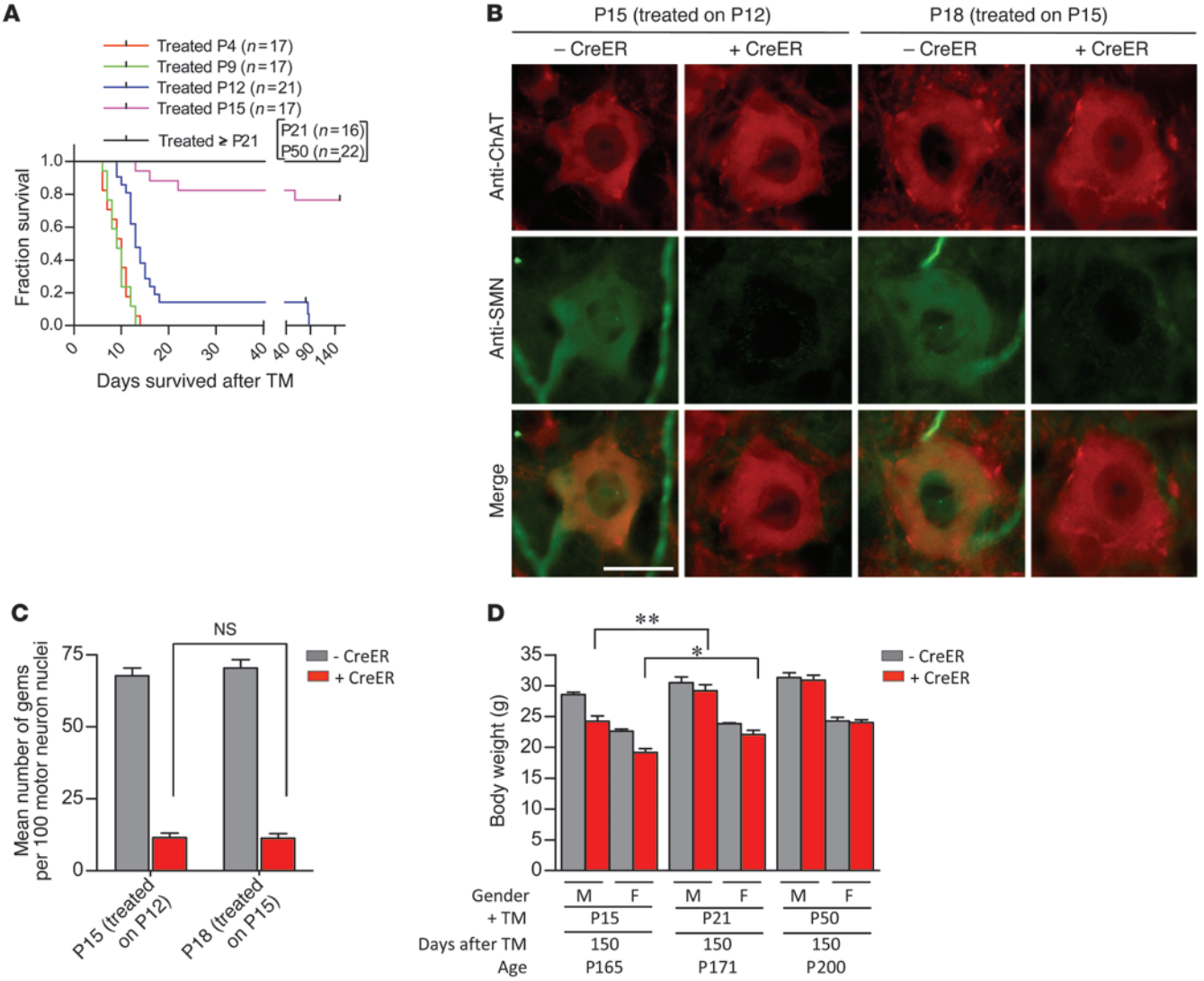

Figure 7

An SMN refractory state emerges concomitant with the establishment of the fully mature neuromuscular synapse. (**A**) Kaplan-Meier curves indicate a dramatic improvement in survival if SMN depletion is effected in mice of P15 or greater. (**B**) Immunostains of motor neurons from P12 and P15 TM-treated mice indicate equivalent low levels of SMN, confirming the efficiency of SMN depletion at the 2 ages. Scale bar: 30 μm. (**C**) Quantification of nuclear gems in motor neurons of the 2 sets of mice did not reveal a difference, confirming equally effective SMN depletion in the 2 cohorts. $n \geq 400$ motor neuron nuclei from $n = 3$ mice of each genotype examined, 1-way ANOVA. (**D**) Analysis of body weights of P15, P21, and P50 TM-treated 2 *SMN2* copy $Smn^{F7/-}$ mice with or without *CreER* indicates small but significant improvement in the phenotypes of mutants depleted of SMN later than P15. $^{*}P < 0.05$; $^{**}P < 0.01$. $n \geq 4$ mice of each genotype, *t* test.

(Figure 5, A, C, and D). To determine whether the injury-induced increase of motor neuronal SMN in normal animals was a consequence of increased transcription, we performed in situ hybridizations of lumbar spinal cord sections from injured, TM-treated *SMN2;*$Smn^{F7/-}$ mice. A probe specific for murine *Smn* detected a significant increase in signal in the ipsilateral versus contralateral motor neurons (Supplemental Figure 10, A and B). Collectively, these results suggest that the cellular processes involved in the regeneration of NMJs alter the requirements for the SMN protein, which peaks as the synapse matures. Thus, there appears to be a particularly stringent requirement for enhanced motor neuronal SMN during the final step(s) of NMJ assembly, following which protein levels decline. Lesions in the *SMN1* gene or, in mouse models, its murine equivalent preclude a sufficient increase in SMN levels and thus prevent efficient regeneration of mature neuromuscular synapses.

Impaired recovery of injured tissue in SMN-depleted mice limited to cells of the neuromuscular system. While it is now clear that motor neurons are an important cellular site of action of the SMN protein (24–26), there is also mounting evidence for a contributing effect of reduced muscle SMN to the SMA phenotype (39–42). Consistent with this notion, we observed evidence of a primary muscle myopathy in aging SMN-depleted 2-copy *SMN2;CreER;*$Smn^{F7/-}$ mice (Figure 3E). To determine whether this phenotype could also be exaggerated in response to injury, TM-treated 2-copy *SMN2;*$Smn^{F7/-}$ mice with or without the *CreER* transgene were

injected in the gastrocnemius muscle at approximately P100 with cardiotoxin, a snake venom–derived polypeptide known to cause myofiber necrosis (43). As expected, necrosis was observed in muscle from both cohorts of mice. We also found that regeneration of the myofibers, determined by quantifying cells with central versus peripheral nuclei, proceeded equally rapidly for about 2 weeks (Figure 6A). However, analysis of the muscle 4 weeks later, at day 42, showed that, whereas tissue from mice with normal SMN had completely recovered, exhibiting similar numbers of central nuclei-containing myofibers relative to the contralateral PBS-injected muscle, muscle from SMN-depleted animals had not. Injured muscle from these mice continued to contain a significantly greater proportion of myofibers with central nuclei (Figure 6, A and B), suggesting an enhanced requirement for muscle SMN in fiber regeneration. Considering the elevated levels of motor neuronal and muscle SMN required during recovery from injury, we asked whether there was a general increase in the requirement for the protein during the regeneration process. Accordingly, we assessed the ability of TM-treated 2-copy *SMN2;Smn*$^{F7/-}$ mice with or without *CreER* to recover from a surface wound to the skin. Interestingly, epithelialization occurred similarly in the 2 cohorts of mice, and wound closure was no different 12 days following trauma (Figure 6, C and D). Moreover, we found no evidence by Western blot analysis of increased SMN expression in skin at the wound site of either set of mice (Figure 6E). These results confirm the notion that the motor neurons and muscle are especially vulnerable to low SMN. The normal development of these cells under conditions of wild-type SMN levels does not endow them with the property of recovering normally in the event of injury or aging once protein is depleted.

An acquired resistance to low SMN concomitant with the transition of the neuromuscular synapse to its fully mature state. Considering the striking difference in phenotypic outcome to depleting SMN during early (P4) versus late (P50) postnatal life, we sought to determine precisely when mice become refractory to low protein. We therefore treated 2-copy *SMN2;CreER;Smn*$^{F7/-}$ mice with TM at P4, -9, -12, -15, -21, and -50 to assess the effects of SMN depletion at these time points on survival, an easily quantifiable and relevant SMA phenotype in murine models. As shown earlier, mice treated at P4 rapidly developed a disease phenotype, succumbing to low SMN approximately 10 days following administration of drug. Delaying SMN depletion to P9 produced no discernible effect on survival, whereas treating mice at P12 enhanced median survival by approximately 4 days. In contrast, delaying protein depletion by an additional 3 days to P15 had an unexpected and quite dramatic effect. Mutants treated at this time point survived, in most instances, to at least 5 months of age (Figure 7A), a greater than 6-fold increase over their P12-treated cohort. To ensure that the altered survival was not simply a consequence of relatively inefficient SMN depletion, spinal cord sections from these mice and their P12-treated cohort were prepared 3 days after TM administration and immunostained with an antibody against the protein. We found that SMN in the motor neuron soma of the 2 sets of mice was equally deficient (Figure 7B). Moreover, nuclear gem numbers in the motor neurons of P15-treated animals were no different from those in P12-treated mice (Figure 7C). Importantly, controls without the *CreER* transgene exhibited robust SMN expression. These results suggest that the altered survival outcome of P15-treated mutants is truly a consequence of their greater age rather than a reduced efficiency of depleting SMN at this later time point.

Consistent with the acquired resistance to low SMN in mice depleted of protein at P15, TM treatment at still later time points (P21 or P50) did not cause death of any of the mutants in the approximate 6-month window during which the mice were examined (Figure 7A). In fact, based on an assessment of body weight 5 months after treatment, delaying SMN depletion to P21 or later mitigated disease to an even greater extent than depletion at P15 (Figure 7D). Collectively, these results suggest that there is a dramatic evolution in the physiology of mice during a 3 day window between approximately P12 and P15 that alters the requirements for SMN, rendering the older animals surprisingly resilient to protein loss. Considering the approximately 5-day delay between initial TM administration and maximum SMN depletion, animals treated at the earlier but not later time point are still undergoing considerable maturation of the neuromuscular synapse when protein concentrations reach disease-causing levels. In other words, the acquisition of the relative resistance to low SMN in the older mutant mice coincides notably with the emergence at approximately P20 of the fully mature neuromuscular synapse (44, 45). This suggests that the relative vulnerability of the organism to low SMN during early postnatal life stems from a specific requirement for the protein in processes involved in NMJ maturation.

Discussion

SMA is a predominantly early-onset disease caused by a deficiency of the SMN protein. Restoring the protein or its critical functions is therefore a logical means to an eventual treatment. This is facilitated to a large extent by the presence in human patients of *SMN2*, a partially functional but nevertheless amenable molecular target. Yet the effectiveness of this, or indeed any, SMA therapy depends on targeting appropriate tissues at the right time during disease progression. We and others previously used mouse models to demonstrate that early augmentation of the SMN protein is necessary to fully mitigate the disease phenotype (17–20, 22). Here, we extend our findings of the temporal requirements for the SMN protein. Our primary observations are as follows: first, we report that the requirements for the protein are radically altered with age. Whereas young animals require relatively high levels of SMN, as determined by the rapid onset of disease following depletion during early postnatal life, adults appear to tolerate much lower levels of the protein. Indeed, SMN depletion in mature animals had a markedly delayed and surprisingly muted effect. Second, we have shown that the relative resistance acquired during adult life to low SMN requires the presence of at least 2 *SMN2* copies. The difference in outcome of depleting protein in adult mice with 1 or 2 *SMN2* genes was notable, indicative of a pronounced threshold effect between the hemizygous and homozygous state. Third, notwithstanding recent reports (ref. 46 and references therein) of severe SMA being a multi-systemic disease, we have confirmed in neonates as well as adults that the adverse effects of low SMN are first seen in the neuromuscular system. This sensitivity, which is detected albeit relatively late in adults depleted of SMN, initially manifests at the NMJ and targets pre- as well as postsynaptic specializations. Fourth, we have demonstrated that the admittedly subtle evidence of neuromuscular pathology in adult mutants becomes pronounced following injury and during regeneration. Consistent with this observation, the reestablishment of mature, functional NMJs triggered a rapid increase in motor neuronal SMN expression. Finally, we have established a relatively narrow window in time during which the organism transitions to an

SMN-refractory state. This transition parallels the emergence of the fully mature NMJ, a likely indication of the critical role SMN plays in establishing the neuromuscular synapse. Collectively, our results argue for an important function of SMN in the maturation and maintenance of the mammalian NMJ and suggest that the most potent concentrations of SMN-inducing agents will be required as the synapse evolves into its fully mature state.

Although it was clear that SMN is needed in early postnatal life to prevent disease onset, the requirement for the protein in mature organisms had not been unequivocally established. In the only attempt we know of to define the postnatal requirements for SMN, adult mice harboring 2 *SMN2* copies were predominantly found to develop disease and perish within a month of removing protein (21). However, in this report, in which only 1 time point was studied, 2 of the relatively small sample size of 7 animals escaped early mortality, making it difficult to unambiguously ascertain how chronic low SMN known to cause severe SMA affects adult health. Considering the initiation of human clinical trials with the first SMN-enhancing agents shown preclinically to be truly potent (www.clinicaltrial.gov; NCT01703988) and the importance of determining whether these agents will have to be administered chronically or not, we sought to systematically address the question by depleting protein levels at multiple postnatal time points. More generally, we anticipated that our experiments would begin to reveal how age might alter spliceosomal requirements, key to proper cell function and a reflection of SMN levels.

Perhaps the most striking outcome of our experiments was discovering how differently neonates and adult mice respond to SMN depletion, and the abruptness with which an SMN-refractory state appeared. Depletion at P4 rapidly resulted in an SMA-like phenotype and mutants perished within 2 weeks, even if they were endowed with 2 *SMN2* copies. In contrast, depleting protein in *SMN2*-homozygous adults (>P21) had a quite muted effect. Although the first result was consistent with the pediatric nature of the human disease and the early onset of a phenotype in SMA model mice, we were surprised by how modestly low protein affected adults. Even more unexpected was the decidedly narrow 3-day window during which animals transitioned, almost completely, from an SMN-sensitive to SMN-resistant state. One alternative could have been an extended period during which mice gradually became resistant to low SMN. Instead, an abrupt transition occurred between mice depleted of protein at P12 and cohorts treated 3 days later. Precisely why the early vulnerability to low SMN ceases at approximately P15 in mice, is not clear. One explanation that is consistent with the effects of low SMN on the NMJs of model mice (23, 24, 47) and human patients (48) lies in the postnatal development of these synapses. In mice, these structures undergo a profound transition during the first 3 weeks of life, evolving from immature "plaques" expressing the slow-conducting embryonic γ-form of the AChR and characterized by imperfectly aligned pre- and postsynaptic regions to elaborately perforated "pretzels" consisting of rapidly conducting adult ε-subunit AChR clusters to which nerve terminals perfectly appose (44, 45). As this process unfolds, an intricate set of signals exchanged among motor neurons, muscle, and terminal Schwann cells initiates the orchestrated assembly of a multitude of molecules at the presynaptic region, the synaptic cleft, and the postsynaptic region (49). In mouse models of SMA, the formation of the NMJs proceeds normally, but their maturation stalls (23). Intriguingly, we found that the transition of the mouse NMJ to its fully mature state is coincidental with the emergence of the SMN-resistant state. What is more, it appears that it is toward the end of the NMJ maturation process — P15 to P20 — that mice become refractory to low SMN, pointing to 1 or more critical functions of the protein in ensuring the transition of this structure to its fully functional adult form. Whether it is through orchestrating snRNP biogenesis and controlling pre-mRNA splicing that SMN regulates the maturation of the neuromuscular synapse is not clear. However, it is interesting to note that the relative activity of SMN in assembling snRNP particles in mouse spinal cord tissue declines precipitously at approximately 2 weeks of age (50), precisely when mutants become relatively unresponsive to low SMN. Future studies cataloguing expression changes in motor neurons and/or muscle as the neuromuscular system matures may be a strategic way for uncovering specific mediators through which SMN regulates this process.

Another notable outcome of our experiments was discovering how selectively low SMN affects the cells of the neuromuscular system. Although it is generally accepted that motor neurons are the first cells to respond adversely to low protein, the direct effects on mutant muscle were unexpected. Acutely low levels of SMN as observed in severe SMA are not generally associated with a primary myopathy, although there is evidence of a role for the protein in the proper development of muscle during fetal stages in mice (41) and 1 report of a myotubular-like myopathy in an unusually severely affected SMA infant (51). Our study was not designed to reveal in utero developmental effects of low SMN on muscle owing to our strategy of depleting protein during postnatal life. Yet it became clear that loss of protein did bring about defects of the muscle that likely originate in a cell-autonomous manner. This was evident in aging animals depleted of SMN and became especially obvious when the muscle was induced to regenerate following traumatic injury. In either instance, the presence of abnormal numbers of myofibers with central nuclei was indicative of an inability of muscle lacking adequate SMN to properly mature. In contrast, the initial ability of the SMN-depleted muscle to respond to injury was found to be normal, as assessed by equivalent numbers of central nuclei–containing fibers in mutants and controls. Together, the results suggest that SMN regulates the final steps in muscle maturation, a process that could well contribute to the restoration of functional NMJs as they turn over during the normal aging process.

In contrast to its effects on muscle, low SMN adversely affected neither the heart nor surface-wound healing. One explanation for our inability to detect cardiac dysfunction, notwithstanding previous reports of such defects, stems from the fact that embryonic and perinatal development in our mice occurred under conditions of normal SMN. In the case of our epithelialization experiments, normal embryonic development does not explain the ability of SMN-depleted skin to regenerate efficiently, since muscle and motor neurons in treated mutants were unable to respond in a similarly appropriate manner. Even if eventual heart dysfunction in SMA is a consequence of constitutive low SMN, the relative vulnerability of the cardiac and neuromuscular systems differs appreciably, since the onset of pathology in the heart of SMN-depleted *CreER;Smn*$^{F7/-}$ mice appeared considerably later than it did at the NMJs of the animals. Collectively, our experiments provide further evidence for the selective vulnerability of the neuromuscular system to low SMN and focus new attention on the effects of the protein in muscle in contributing to the disease phenotype.

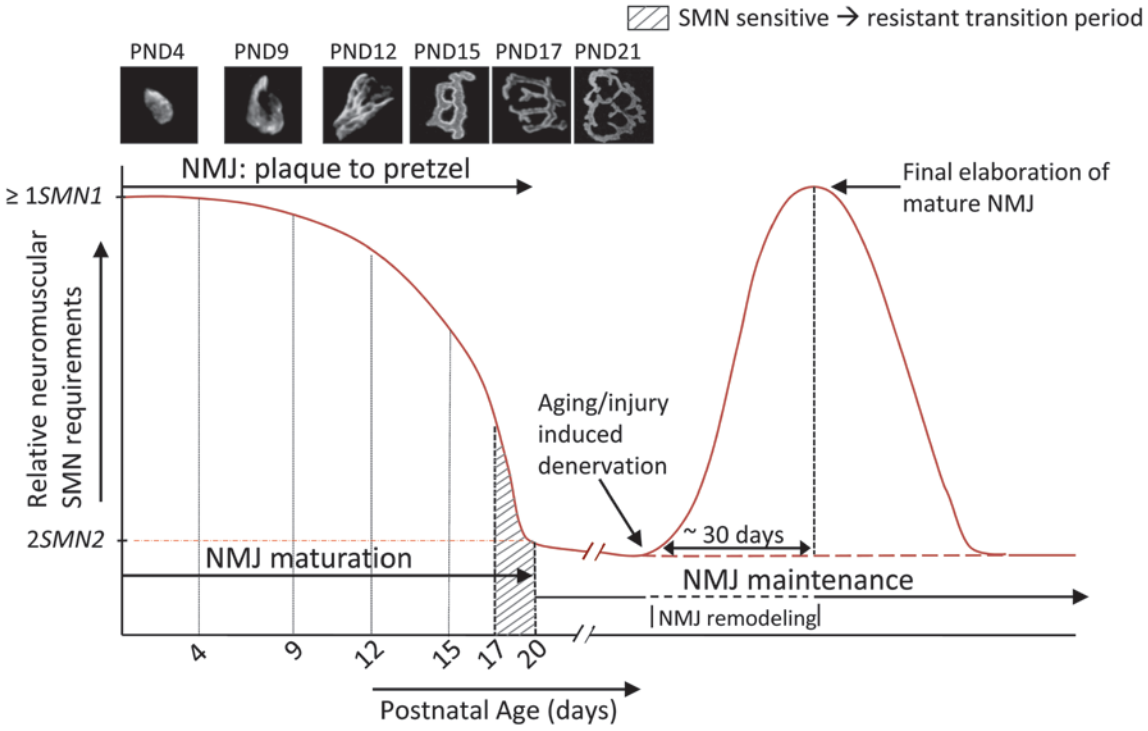

Figure 8
A model encapsulating the postnatal requirement for the SMN protein in the murine model. The requirement for the protein is adequately met by 1 or more *SMN1* copies or *SMN2* copies that, between them, express equivalent levels of the protein. This requirement is at its greatest during the neonatal period encompassing NMJ refinement and maturation. It eventually falls by approximately P20, a time point defined by the establishment of the fully mature neuromuscular synapse (see photomicrographs), to levels that are satisfied by 2 *SMN2* copies. In the approximately 3-day window prior to this time point, mice become relatively resistant to low SMN. Injury of the NMJ during aging or trauma is accompanied by a surge in demand for the protein, specifically in tissues of the neuromuscular system, which is not adequately met by 2 *SMN2* copies. The enhanced requirement appears to peak as the NMJ matures and brings about, in SMN-depleted mutants, an inability to fully repair the neuromuscular synapse. Thus, SMN is thought to play 2 related roles at the neuromuscular synapse — its initial maturation and its continued maintenance. Note: figure not drawn to scale.

Our results also provide the clearest basis yet for the arrest in NMJ maturation under conditions of low SMN. This stems from the observation that disruption of neuromuscular synapses triggers an increase in motor neuronal SMN expression that peaks during the final events of NMJ maturation. Others have also noted perturbations in NMJ remodeling (52), but did not correlate it with changes in SMN expression, a unique finding of this study and one that distinguishes it from prior reports (23–25). Our results suggest that there is an enhanced demand for SMN initially in *all* motor neurons and/or muscle as the neuromuscular system matures and a later surge in individual cells as NMJs turn over and have to be replaced as part of the normal aging process (Figure 8). *SMN2* alone fails to meet this demand, preventing the initial maturation of the neuromuscular synapses and eventually compromising the maintenance of this structure. We conclude that SMN-enhancing agents will be most effective in thwarting the neuromuscular SMA phenotype if administered prior to the normal emergence of the mature NMJ. We further predict that following transition of the neuromuscular synapse to its mature state and barring severe injury to its constituent cells, the concentrations of SMN-inducing drug(s) administered to patients may be reduced without triggering severe disease. More generally, if it can be determined that NMJ defects in SMA stem from the incorrect splicing of specific genes, it will provide important evidence for the changing requirements for spliceosomal activity at least in the proper assembly of this synapse as the organism matures.

The mouse model we describe provides a unique tool to investigate specific mediators of the SMN-based NMJ phenotype.

Methods

Mice

To generate inducible *Smn* mice harboring 0, 1, or 2 *SMN2* copies, we initially bred homozygous *SMN2*$^{+/+}$;*Smn*$^{+/-}$ animals (ref. 9; Jax stock no. 005024; The Jackson Laboratory) with a line (*Smn*$^{F7/+}$) harboring an allele of the murine *Smn* gene that contains loxP sites flanking exon 7 (ref. 30; Jax stock no. 006138; The Jackson Laboratory). Upon Cre expression, the loxP sites recombine irreversibly, thereby deleting exon 7 and inactivating the allele. We simultaneously bred the *SMN2* homozygous carriers with a transgenic line (*CreER;Smn*$^{+/+}$) bearing a TM-inducible *CreER* allele (ref. 32; Jax stock no. 004682; The Jackson Laboratory). Progeny mice (*SMN2*$^{+/-}$;*Smn*$^{F7/-}$ and *SMN2*$^{+/-}$;*CreER;Smn*$^{+/-}$) from the 2 crosses were then interbred to generate *CreER;Smn*$^{F7/-}$ mutants harboring variable copies of the *SMN2* gene. All experiments described in this study included both male and female mice. To preclude strain background effects, littermate controls were used in all experiments.

TM treatment

A stock solution of 20 mg/ml TM (Sigma-Aldrich) was prepared in corn oil, and a 100 mg/kg dose of this solution was administered to mice by oral gavage for 3 consecutive days. Where appropriate, controls were administered corn oil alone.

Genotyping

Mice were genotyped by PCR using DNA from tail tissue. Detailed protocols have been previously described (9, 30, 32, 53). The following primers were used for the various alleles: *CreER* — (forward; 5′-GCTAAGTGCCTTCTCTACACCTGC–3′, reverse; 5′-GGAAAATGCTTCTGTCCGTTTG-3′), *SMN2* – (forward; 5′-CTGACCTACCAGGGATGAGG–3′, reverse; 5′-GGTCTGTTCTACAGCCACAGC-3′), Smn^{F7} allele – (forward; 5′-gctAAGTGCCTTCTCTACACCTGC-3′, reverse; 5′-GGAAAATGCTTCTGTCCGTTTG-3′). The Smn^{F7} primers enabled us to determine zygosity of the allele — a single 635-bp band for $Smn^{F7/F7}$ mice and an additional 435-bp band for $Smn^{F7/-}$ mutants. *SMN2* zygosity was determined using a multiplex PCR described in a previous report (53)

EMGs

The emergence of fibrillation potentials was examined by needle EMG in anesthetized mice. The data were collected from the gastrocnemius muscle (1 minute of recording per insertion × 3 points), and analyzed with a Viking IV EMG machine (Viasys; Nicolet Biomedical). The recording conditions were set as follows: gain, × 1,000; low cut, 400 Hz; high cut, 1.5 kHz; notch filter, 60 Hz. As a positive control, the right-sciatic nerve of Ntg mice was transected under anesthesia, the skin sutured, and EMGs performed a week later on both ipsilateral and contralateral gastrocnemii.

Tissue injury paradigms

To determine how SMN-depleted muscle responded to traumatic injury, mice were anesthetized with 1%–2% isoflurane, the gastrocnemius muscle exposed, and a 30-gauge needle used to inject 20 μl of a 10 μM solution of cardiotoxin in PBS into the belly of the muscle. The wound was subsequently sutured and muscle from the mice examined at the time points described in Results. To assess the ability of SMN-depleted mice to remodel NMJs, the right sciatic nerve was exposed under anesthesia and then crushed for 5 seconds with a pair of fine forceps. The wound was closed and NMJs in the gastrocnemius examined 6, 18, 30, and 42 days later. To ensure consistency between animals, the lesion was always made 40 mm from the tip of the third digit. To ascertain the epithelialization process in the mice, 25 mm^2 (5 mm × 5 mm) of skin was removed from the right hip of anesthetized, depilated mice, and subsequent recovery assessed at day 6 and 12 after injury.

Blood chemistry

Mice were euthanized with CO_2 gas and approximately 700 μl aspirated from the right ventricle using a 21-gauge needle. Differential blood cell counts were carried out on 20 μl of this blood using an automatic hemocytometer FORCYTE (Oxford Science Inc.). The remainder was immediately transferred to a BD Microtainer Serum Separator Tube (BD), spun at 5900 *g* for 8 minutes, and the serum (~350 μl) stored at –80°C until analyzed for levels of serum proteins at the Oriental Yeast Company.

Cardiopulmonary function

Adult mice were anesthetized with 1%–2% isoflurane to maintain a heart rate of 500 bpm. After depilating the chest area, the mice were placed on a heating pad to maintain a constant body temperature of 37°C. Echocardiography was performed using the Vevo770 imaging system (VisualSonics) equipped with a 30-MHz transducer. B-mode and M-mode images were obtained in the parasternal short-axis view. LV end-diastolic (LVEDD) and LV end-systolic dimensions (LVESD) were measured at the midpapillary muscle level. LV fractional area changes (FAC%) were calculated as (end-diastolic area – end-systolic area/end-diastolic area) × 100. Cardiac index (ml/min/g) was calculated using the following formula: [7.0LVEDD3/(2.4 + LVEDD) – 7.0LVESD3/(2.4 + LVESD)] × heart rate/1000} ÷ body weight. Heart rate and arterial hemoglobin saturation (SpO_2) was ascertained in conscious mice on the heating pad. Movement of the mice was restricted by placing cardboard on either side of the animals and occluding their vision with black paper. The proximal tail was then cuffed with a pulse oximeter probe (MouseOxW; Starr Life Sciences Corp.) and parameters measured in a quiet room for 60 minutes. The data were averaged from values collected every 0.2 seconds over a 30-second period.

Motor behavior assays

Vertical pole test. This test employed a modified version of the protocol previously described by Matsuura et al. (54). Briefly, mice were placed in the center of a vertically positioned metal pole (60 cm long, 1 cm diameter) and covered with a mesh tape, with their snouts oriented toward the ceiling. Motor performance was measured by the latency to turn around in order to descend the pole. Each animal was subjected to 10 trials and a motor defect noted when a mouse was unable to turn around within 30 seconds in any of the trials. The disease was defined as phenotypically discernible if a mouse performed in a similar manner on 2 consecutive days. The 30 second cut-off time was chosen based on a 100% success rate in age-matched control mice (n = 50).

Rotarod analysis. The rotarod test was performed using a machine from Columbus Instruments under conditions of constant (20 rpm) velocity. Mice were subjected to 10 trials following 3 training periods of 1 minute each. An inability to remain on the rotating rod for at least 30 seconds in each of the trials constituted a motor defect. A similar performance the following day was required to confirm disease onset.

Grip strength. Forelimb grip strength was measured using the BIOSEB Grip Strength Tester BIO-GS3. Mice were allowed to grasp the bar of the tester and pulled by the tail away from it until their grip was broken. The force applied at the moment of release was recorded by the machine as the maximal grip strength. Each mouse was subjected to 6 trials and the mean reported for the analysis.

Righting ability. This test was administered as previously described (23) to estimate muscle strength of early postnatal mice. Briefly, pups were turned over onto their backs and latency to stably place all 4 paws on the bench top was recorded. The following arbitrary scores, previously employed by us (23), were used to quantify impaired righting ability: 5 for 0–2 seconds righting ability, 4 for 3–5 seconds, 3 for 6–10 seconds, 2 for 11–30 seconds, 1 for 31–60 seconds, and 0 if more than 61 seconds. The procedure was repeated 6 times for each animal, and the sum of the scores was designated as the righting ability score.

Hind limb motor performance. The test was administered using a previously published (55) scale that rated 2 criteria: (A) walking with hind limbs and (B) the placing/stepping reflex. Scores for each of the criteria were assigned as follows: (A) walking: 0, normal; 1, toes flat under body when walking but ataxia present; 2, knuckle walking; 3, movements in hind limbs but unable to walk; and 4, no hind limb movement/drags hind limbs; (B) placing/stepping reflex: 0, normal; 1, weak; and 2, no stepping. The experiment was repeated thrice and average scores from each of the 2 criteria summed to arrive at a final estimate.

Weight/survival. Survival of mice was determined by noting the day on which a mouse succumbed to the disease or had to be euthanized due to disease conditions, such as poor response to touch, a failure to

eat/drink, inability to groom, or 20% or greater loss of body weight. In pups, the appearance of cyanosis was deemed sufficient for euthanasia. Survival data were plotted as Kaplan-Meier curves. Mice were weighed as required.

In situ hybridization

Templates for the antisense RNA probes were prepared by reverse transcribing RNA from a wild-type mouse and amplifying murine *Smn* using the following primers: forward, 5′-CGGAGCGGGCTCCGAGCAGGAAGATA-3′ (mouse *Smn* exon 1 sequence); reverse, 5′-ATTTAGGTGACACTATAGtatgtgagcactttccttc-3′ (upper case letters indicate SP6 RNA polymerase recognition sequence; lower case letters indicate sequence specific to murine *Smn* exon 7). After purifying the PCR product with a QIAQuick Gel Extraction Kit (QIAGEN), digoxigenin-labeled (DIG-labeled) RNA probes were prepared using DIG RNA Labeling Mix (Roche) according to the manufacturer's instructions. In situ hybridizations were performed as previously described (56). DAPI was used to visualize nuclei. *Smn* transcript levels were assessed after imaging the spinal cord sections (×400, Nikon Eclipse, E80i), converting the images to grayscale, and measuring staining intensities using the ImageJ (NIH) software program. Spinal motor neurons were identified based on their anatomical localization and the presence of a large nucleus that stained relatively faintly with DAPI. Thirty or more ipsilateral as well as contralateral motor neurons within the L6–S1 segments were analyzed for this experiment.

Analysis of cellular pathology

Spinal motor neuron and muscle histology. Skeletal muscle pathology was investigated in the gastrocnemius. Animals were euthanized and whole muscle dissected, oriented in Tissue-Tek OCT embedding media (Fisher Scientific) for cross-sectional analysis, and flash-frozen in liquid nitrogen–cooled (N_2) isopentane. Transverse sections (8-μm thick) from the belly of the muscle were cut on a cryostat (Leica) and the sections stained with H&E (Sigma-Aldrich) to examine fiber morphology as previously described (57). Fiber size was determined using SPOT v4.5 software (Diagnostic Instruments) following image acquisition of the stained sections. Cardiac muscle pathology was similarly assessed from transverse sections cut at the level of the ventricles. Immunostains on muscle were performed on 8-μm–thick sections of tissue that were flash frozen as described above. The sections were fixed in 100% methanol (4°C, 20 minutes), blocked (3% BSA, 2% Triton-X 100) for 20 minutes (room temperature), and then incubated with an anti-SMN antibody, (7F3, 1:40, ref. 58) dissolved in saline. After washing, the sections were incubated in appropriate fluorescently conjugated secondary antibodies (24 hours at 4°C), overlaid with a mixture of DAPI and mounting media (Vectashield), and imaged on an E80i Nikon microscope equipped with a Spot Flex digital camera (Diagnostic Instruments).

To determine spinal motor neuron and gem counts and to assess motor neuron morphology, spinal cord tissue was extracted from mice following transcardial perfusion with 1× PBS and then 4% PFA. Following postfixation in 4% PFA (4°C for 4 hours), tissue was cryoprotected (30% sucrose for 3 days at 4°C), embedded in Tissue-Tek OCT, and then frozen in liquid N_2–cooled isopentane for sectioning. 20-mm transverse sections from lumbar spinal cord were cut and stained as described above except for the additional use of an antibody against choline acetyltransferase (ChAT) (1:100; Millipore). Motor neuron numbers were assessed in 8 sections of each of 3 (L5–L6) lumbar segments and the raw number extrapolated to the entire region based on the length and thickness of each section. Gem numbers were determined by counting intranuclear SMN-positive dot-like structures within ChAT-expressing motor neurons. Motor neuronal cytoplasmic SMN levels were determined by assessing the fluorescence intensity of the entire motor neuron and subtracting from it the fluorescence of the nucleus.

Cytoarchitecture of NMJs. The analysis of NMJ cytoarchitecture was essentially carried out as previously described (22). In pups and young mice, the extent of presynaptic pathology was determined by the presence of swollen, neurofilament-filled end-bulb structures. Postsynaptic defects were quantified based on fragmented and poorly staining AChR clusters. Abnormalities of adult NMJs were defined by disassembled AChR clusters, poorly branched nerve terminals, and incomplete overlap between pre- and postsynaptic regions. To describe NMJ remodeling following nerve injury, pre- and postsynaptic regions were classified into 1 of 4 categories each (also see Results and Supplemental Figure 6A). All of the NMJ analyses were performed on 300 or more NMJs from each mouse.

Western blotting

SMN protein levels in the various cohorts of mice were determined by Western blot analysis using standard procedures described previously (9). SMN (1:10,000; BD Biosciences) and α-tubulin (1:1600; Sigma-Aldrich) monoclonal antibodies were visualized using the ECL Detection Kit (RPN 2109; GE Healthcare). Quantification of band intensities was performed using ImageJ software (NIH).

Statistics

Kaplan-Meier survival curves were compared and assessed for differences using the log-rank test equivalent to the Mantel-Haenszel test. The unpaired 2-tailed Student's *t* test or 1-way ANOVA followed by Tukey's post hoc comparison, where indicated, was used to compare means for statistical differences. Data in the manuscript are represented as mean ± SEM unless otherwise indicated. $P < 0.05$ was considered significant. Statistical analyses were performed with GraphPad Prism v4.0 (GraphPad Software).

Study approval

All experiments were conducted in accordance with the protocols described in the *Guide for the Care and Use of Laboratory Animals* (NIH. Revised 2011) and were approved by Columbia University's Institutional Laboratory Animal Care and Use Committees.

Acknowledgments

We thank D.C. De Vivo and L. Pellizzoni for their advice and for the many suggestions proffered while performing this work. We are also grateful to C.E. Henderson for his advice, thoughts, and comments on the manuscript. The 7F3 antibody was a generous gift from the Pellizzoni laboratory. This study was supported by Association Française Contre Les Myopathies (AFM) and SMA Europe grants to U.R. Monani and S. Kariya. Additionally, U.R. Monani was supported by the Muscular Dystrophy Association, Department of Defense grant W81XWH-11-1-0753, Families of SMA, and NIH R01 NS057482. T. Obis was funded by a grant from the Catalan Government (Generalitat) (2009SGR01248) and the Rovira i Virgili University (2010BRDI-06-18).

Received for publication July 8, 2013, and accepted in revised form October 31, 2013.

Address correspondence to: Umrao R. Monani, P&S, Room 5-422, 630 W. 168th St., New York, New York 10032, USA. Phone: 212.342.5132; Fax: 212.342.4512; E-mail: um2105columbia.edu.

1. Lefebvre S, et al. Identification and characterization of a spinal muscular atrophy-determining gene. *Cell*. 1995;80(1):155–165.
2. Monani UR. Spinal muscular atrophy: a deficiency in a ubiquitous protein; a motor neuron-specific disease. *Neuron*. 2005;48(6):885–896.
3. Burghes AH, Beattie CE. Spinal muscular atrophy: why do low levels of survival motor neuron protein make motor neurons sick? *Nat Rev Neurosci*. 2009;10(8):597–609.
4. Lorson CL, Hahnen E, Androphy EJ, Wirth B. A single nucleotide in the SMN gene regulates splicing and is responsible for spinal muscular atrophy. *Proc Natl Acad Sci U S A*. 1999;96(11):6307–6311.
5. Monani UR, et al. A single nucleotide difference that alters splicing patterns distinguishes the SMA gene SMN1 from the copy gene SMN2. *Hum Mol Genet*. 1999;8(7):1177–1183.
6. Kashima T, Manley JL. A negative element in SMN2 exon 7 inhibits splicing in spinal muscular atrophy. *Nat Genet*. 2003;34(4):460–463.
7. Coovert DD, et al. The survival motor neuron protein in spinal muscular atrophy. *Hum Mol Genet*. 1997;6(8):1205–1214.
8. Lefebvre S, et al. Correlation between severity and SMN protein level in spinal muscular atrophy. *Nat Genet*. 1997;16(3):265–269.
9. Monani UR, et al. The human centromeric survival motor neuron gene (SMN2) rescues embryonic lethality in Smn(–/–) mice and results in a mouse with spinal muscular atrophy. *Hum Mol Genet*. 2000;9(3):333–339.
10. Hsieh-Li HM, et al. A mouse model for spinal muscular atrophy. *Nat Genet*. 2000;24(1):66–70.
11. McAndrew PE, et al. Identification of proximal spinal muscular atrophy carriers and patients by analysis of SMNT and SMNC gene copy number. *Am J Hum Genet*. 1997;60(6):1411–1422.
12. Feldkotter M, Schwarzer V, Wirth R, Wienker TF, Wirth B. Quantitative analyses of SMN1 and SMN2 based on real-time lightCycler PCR: fast and highly reliable carrier testing and prediction of severity of spinal muscular atrophy. *Am J Hum Genet*. 2002;70(2):358–368.
13. Burnett BG, Crawford TO, Sumner CJ. Emerging treatment options for spinal muscular atrophy. *Curr Treat Options Neurol*. 2009;11(2):90–101.
14. Lorson MA, Lorson CL. SMN-inducing compounds for the treatment of spinal muscular atrophy. *Future Med Chem*. 2012;4(16):2067–2084.
15. Hua Y, et al. Peripheral SMN restoration is essential for long-term rescue of a severe spinal muscular atrophy mouse model. *Nature*. 2011;478(7367):123–126.
16. Porensky PN, et al. A single administration of morpholino antisense oligomer rescues spinal muscular atrophy in mouse. *Hum Mol Genet*. 2012; 21(7):1625–1638.
17. Foust KD, et al. Rescue of the spinal muscular atrophy phenotype in a mouse model by early postnatal delivery of SMN. *Nat Biotechnol*. 2010;28(3):271–274.
18. Passini MA, et al. CNS-targeted gene therapy improves survival and motor function in a mouse model of spinal muscular atrophy. *J Clin Invest*. 2010;120(4):1253–1264.
19. Duque S, et al. Intravenous administration of self-complementary AAV9 enables transgene delivery to adult motor neurons. *Mol Ther*. 2009; 17(7):1187–1196.
20. Valori CF, et al. Systemic delivery of scAAV9 expressing SMN prolongs survival in a model of spinal muscular atrophy. *Sci Transl Med*. 2010; 2(35):35ra42.
21. Le TT, et al. Temporal requirement for high SMN expression in SMA mice. *Hum Mol Genet*. 2011;20(18):3578–3591.
22. Lutz CM, et al. Postsymptomatic restoration of SMN rescues the disease phenotype in a mouse model of severe spinal muscular atrophy. *J Clin Invest*. 2011;121(8):3029–3041.
23. Kariya S, et al. Reduced SMN protein impairs maturation of the neuromuscular junctions in mouse models of spinal muscular atrophy. *Hum Mol Genet*. 2008;17(16):2552–2569.
24. Kong L, et al. Impaired synaptic vesicle release and immaturity of neuromuscular junctions in spinal muscular atrophy mice. *J Neurosci*. 2009; 29(3):842–851.
25. Ling KK, Lin MY, Zingg B, Feng Z, Ko CP. Synaptic defects in the spinal and neuromuscular circuitry in a mouse model of spinal muscular atrophy. *PLoS One*. 2010;5(11):e15457.
26. Park GH, Maeno-Hikichi Y, Awano T, Landmesser LT, Monani UR. Reduced survival of motor neuron (SMN) protein in motor neuronal progenitors functions cell autonomously to cause spinal muscular atrophy in model mice expressing the human centromeric (SMN2) gene. *J Neurosci*. 2010;30(36):12005–12019.
27. Le TT, et al. SMNDelta7, the major product of the centromeric survival motor neuron (SMN2) gene, extends survival in mice with spinal muscular atrophy and associates with full-length SMN. *Hum Mol Genet*. 2005;14(6):845–857.
28. Bromberg MB, Swoboda KJ. Motor unit number estimation in infants and children with spinal muscular atrophy. *Muscle Nerve*. 2002;25(3):445–447.
29. Swoboda KJ, et al. Natural history of denervation in SMA: relation to age, SMN2 copy number, and function. *Ann Neurol*. 2005;57(5):704–712.
30. Frugier T, et al. Nuclear targeting defect of SMN lacking the C-terminus in a mouse model of spinal muscular atrophy. *Hum Mol Genet*. 2000;9(5):849–858.
31. Schrank B, et al. Inactivation of the survival motor neuron gene, a candidate gene for human spinal muscular atrophy, leads to massive cell death in early mouse embryos. *Proc Natl Acad Sci U S A*. 1997;94(18):9920–9925.
32. Hayashi S, McMahon AP. Efficient recombination in diverse tissues by a tamoxifen-inducible form of Cre: a tool for temporally regulated gene activation/inactivation in the mouse. *Dev Biol*. 2002;244(2):305–318.
33. Park GH, Kariya S, Monani UR. Spinal muscular atrophy: new and emerging insights from model mice. *Curr Neurol Neurosci Rep*. 2010;10(2):108–117.
34. Bevan AK, et al. Early heart failure in the SMNDelta7 model of spinal muscular atrophy and correction by postnatal scAAV9-SMN delivery. *Hum Mol Genet*. 2010;19(20):3895–3905.
35. Shababi M, Habibi J, Yang HT, Vale SM, Sewell WA, Lorson C. Cardiac defects contribute to the pathology of spinal muscular atrophy models. *Hum Mol Genet*. 2010;19(20):4059–4071.
36. Heier CR, Satta R, Lutz C, DiDonato CJ. Arrhythmia and cardiac defects are a feature of spinal muscular atrophy model mice. *Hum Mol Genet*. 2010;19(20):3906–3918.
37. Rudnik-Schöneborn S, et al. Congenital heart disease is a feature of severe infantile spinal muscular atrophy. *J Med Genet*. 2008;45(10):635–638.
38. Valdez G, et al. Attenuation of age-related changes in mouse neuromuscular synapses by caloric restriction and exercise. *Proc Natl Acad Sci U S A*. 2010;107(33):14863–14868.
39. Guettier-Sigrist S, et al. On the possible role of muscle in the pathogenesis of spinal muscular atrophy. *Fundam Clin Pharmacol*. 2001;15(1):31–40.
40. Arnold AS, et al. Reduced expression of nicotinic AChRs in myotubes from spinal muscular atrophy I patients. *Lab Invest*. 2004;84(10):1271–1278.
41. Hayhurst M, Wagner AK, Cerletti M, Wagers AJ, Rubin LL. A cell-autonomous defect in skeletal muscle satellite cells expressing low levels of survival of motor neuron protein. *Dev Biol*. 2012;368(2):323–334.
42. Mutsaers CA, et al. Reversible molecular pathology of skeletal muscle in spinal muscular atrophy. *Hum Mol Genet*. 2011;20(22):4334–4344.
43. Ownby CL, Fletcher JE, Colberg TR. Cardiotoxin 1 from cobra (Naja naja atra) venom causes necrosis of skeletal muscle in vivo. *Toxicon*. 1993;31(6):697–709.
44. Sanes JR, Lichtman JW. Induction, assembly, maturation and maintenance of a post-synaptic apparatus. *Nat Rev Neurosci*. 2001;(11):791–805.
45. Shi L, Fu AKY, Ip NY. Molecular mechanisms underlying maturation and maintenance of the vertebrate neuromuscular junction. *Trends Neurosci*. 2012;35(7):441–453.
46. Hamilton G, Gillingwater TH. Spinal muscular atrophy: going beyond the motor neuron. *Trends Mol Med*. 2013;19(1):40–50.
47. Murray LM, Comley LH, Thomson D, Parkinson N, Talbot K, Gillingwater TH. Selective vulnerability of motor neurons and dissociation of pre- and post-synaptic pathology at the neuromuscular junction in mouse models of spinal muscular atrophy. *Hum Mol Genet*. 2008;17(7):949–962.
48. Martínez-Hernández R, et al. Synaptic defects in type I spinal muscular atrophy in human development. *J Pathol*. 2013;229(1):49–61.
49. Wu H, Xiong WC, Mei L. To build a synapse: signaling pathways in neuromuscular junction assembly. *Development*. 2010;137(7):1017–1033.
50. Pellizzoni L. Chaperoning ribonucleoprotein biogenesis in health and disease. *EMBO Rep*. 2007;8(4):340–345.
51. Nadeau A, D'Anjou G, Debray G, Robitaille Y, Simard LR, Vanasse M. A newborn with spinal muscular atrophy type 0 presenting with a clinicopathological picture suggestive of myotubular myopathy. *J Child Neurol*. 2007;22(11):1301–1304.
52. Murray LM, Beauvais A, Bhanot K, Kothary R. Defects in neuromuscular junction remodelling in the Smn(2B/–) mouse model of spinal muscular atrophy. *Neurobiol Dis*. 2012;49C:57–67.
53. Gogliotti RG, Lutz C, Jorgensen M, Huebsch K, Koh S, Didonato CJ. Characterization of a commonly used mouse model of SMA reveals increased seizure susceptibility and heightened fear response in FVB/N mice. *Neurobiol Dis*. 2011;43(1):142–151.
54. Matsuura K, Kabuto H, Makino H, Ogawa N. Pole test is a useful method for evaluating the mouse movement disorder caused by striatal dopamine depletion. *J Neurosci Methods*. 1997;73(1):45–48.
55. Marsala M, Yaksh TL. Transient spinal ischemia in the rat: characterization of behavioral and histopathological consequences as a function of the duration of aortic occlusion. *J Cereb Blood Flow Metab*. 1994;14(3):526–535.
56. Schaeren-Wiemers N, Gerfin-Moser A. A single protocol to detect transcripts of various types and expression levels in neural tissue and cultured cells: in situ hybridization using digoxigenin-labelled cRNA probes. *Histochemistry*. 1993;100(6):431–440
57. Monani UR, et al. A transgene carrying an A2G missense mutation in the SMN gene modulates phenotypic severity in mice with severe (type I) spinal muscular atrophy. *J Cell Biol*. 2003;160(1):41–52.
58. Carissimi C, et al. Unrip is a component of SMN complexes active in snRNP assembly. *FEBS Lett*. 2005;579(11):2348–2354.